Peptide-Mediated Targeting Mesoporous Silica Nanoparticles: A Novel Tool for Fighting Bladder Cancer

Sean K. Sweeney[1, †] PhD, Yi Luo[2] PhD, Michael A. O'Donnell[2] MD, and Jose G. Assouline[1, *, †] PhD

[1] Department of Biomedical Engineering, University of Iowa, 1402 Seamans Center for the Engineering Arts and Sciences, Iowa City, IA 52242, USA; NanoMedTrix, LLC 2500 Crosspark Road, Suite E119 Coralville, IA 52241-4710, USA
[2] Department of Urology, University of Iowa, Roy J. and Lucille A. Carver College of Medicine, Iowa City, IA 52242, USA

Transitional cell carcinoma of the bladder is particularly devastating due to its high rate of recurrence and difficulty in retention of treatments within the bladder. Current cystoscopic approaches to detect and stage the tumor are limited by the penetrative depth of the cystoscope light source, and intravesical dyes that highlight tumors for surgical resection are non-specific. To address the needs for improved specificity in tumor detection and follow-up, we report on a novel technology relying on the engineered core of mesoporous silica (MSN) with surface modifications that generate contrast in fluorescence and magnetic resonance imaging (MRI). The particle surface was further functionalized to include a bladder cancer cell specific peptide, Cyc6, identified via phage display. This peptide possesses nanomolar specificity for bladder cancer cells and homology across multiple species including mouse, canine, and human. Our study takes advantage of its target expression in bladder tumor which is not expressed in normal bladder wall. When functionalized to MSN, the Cyc6 improved binding efficiency and specificity for bladder cancer cells *in vitro*. In an *in vivo* model, MSN instilled into bladders of tumor-bearing mice enhanced T_1- and T_2-weighted MRI signals, improving the detection of the tumor boundaries. These findings support the notion that our targeted nanomaterial presents new options for early detection and eventual therapeutic intervention. Ultimately, the combination of real-time and repeated MRI evaluation of the tumors enhanced by nanoparticle contrast have the potential for translation into human clinical studies for tumor staging, therapeutic monitoring, and drug delivery.

KEYWORDS: *Mesoporous Silica Nanoparticles, Transitional Cell Carcinoma, Bladder, Magnetic Resonance Imaging, Cystoscopy, Mouse Orthotopic Tumor Model, Phage Display Library.*

INTRODUCTION

Transitional Cell Carcinoma (TCC) of the bladder affects more than 74,000 new patients in the United States and with over 15,000 deaths predicted for 2016, it accounts for almost 5% of all tumors diagnosed[1] and an estimated $4.7 billion annual cost.[2] Much of this cost (monetary, pain and suffering) is associated with the long-term screening following therapy. Initial screening for bladder cancer is warranted when patients present with hematuria (blood in urine), pain in the back or pelvis, or painful urination. Chief among the impetus to find better screening methods is that, although the majority of human bladder cancer is superficial at the time of detection, the recurrence rate and the risk of progression to advanced disease are high.[3–8] Bladder cancer is currently screened for using a cystoscopic approach. White light cystoscopy simply illuminates the bladder for a visual examination of the inner wall,[9] while fluorescent or narrow band cystoscopy involves the use of broad, non-specific fluorescent dyes to aid in differentiating the tumor from normal bladder epithelium.[10–12] Rather than targeting a particular marker for bladder cancer, these generic labeling methods colorize the entire bladder wall with some differential highlighting taking place. This approach can be effective for identifying relatively large tumors, but small lesions may still be missed.[13, 14] In addition, cystoscopic staging of the tumor is impossible due to the superficiality of the visualization; biopsies are still required to identify the depth of penetration of the tumor.[15, 16]

Given the public health importance of this devastating disease, new and technically advanced methods are slow

to emerge and must be expedited. A number of accepted approaches are used clinically including: transurethral resection and attenuated bacillus Calmette-Guerin (BCG) immunotherapy. However these methods have recurrence rates of up to 70%[4, 6, 8] and 50%,[3, 5, 7] respectively. Injection of BCG is fraught with technical pitfalls, laden with pain and prone to cause major urinary tract infections (UTI) which may lead to sepsis and death.[17, 18]

Other nanoparticle treatments have been attempted for use in bladder cancer, with mixed results.[19–24] For example, because BCG immunotherapy is contraindicated in a significant proportion of patients who are immunocompromised, groups have packaged attenuated forms of BCG into nanoparticles for delivery.[19, 22] Unfortunately, these have proven to be less effective at stimulating an immune response than the live form of the bacteria. Nanoparticles based on gold and other biocompatible metals have been used for photothermal therapy, in which emitted light causes a cytotoxic release of thermal energy.[23, 24] By the nature of their mode of action, these types of particles require extreme specificity to destroy only tumor cells and leave normal epithelia unharmed. Many forms of nanoparticles are used as carriers of chemotherapeutics;[20, 21] these, however, often cannot be visualized/detected and have poor retention in the bladder. Thus it is clear that any diagnostic or therapeutic to be used in the bladder must
(1) react quickly with the bladder cancer, and
(2) be retained through multiple cycles of bladder filling and emptying.

Previously, we have developed a nano-based technology which lays the groundwork for the proof-of-concept of our MSN as a tool for labeling bladder cancer through *in vitro* and *in vivo* studies.[25] The design and manufacture of the multifunctional mesoporous silica nanoparticle (MSN) was carried out with the express purpose of being biocompatible and non-toxic. Thus, individual components were chosen which would maintain biocompatibility in the final form. The silica core is largely bioinert; studies to determine the toxicity of MSN injected intravenously found a lethal dose (LD_{50}) of more than 1 g/kg, far higher than any dose needed for imaging studies.[26] Another group found the viability remained high (>90%) in endothelial cell cultures at exposures above 100 μg/mL.[27] The Gd_2O_3 component is far less reactive than free Gd^{3+} ions, which are still clinically permitted in most cases in the form of chelates.[28, 29] Fluorophores (FITC/TRITC) are used clinically as tracer dyes for various procedures,[30, 31] and poly(ethylene glycol) (PEG) is a common ingredient in mild laxatives, though at much higher concentrations.[32] Furthermore, it is important to note that the bladder epithelium is mostly non-reactive with respect to absorption of material into the bloodstream; only 3–4% of low molecular weight chemotherapeutics injected into the bladder typically enter the circulation.[33–35]

Our manufactured MSN were previously found to preferentially bind bladder cancers *in vivo* relative to normal bladder epithelium. In order to further improve binding and retention of particles, we introduce an additional functionalization of the particle with a bladder cancer cell specific peptide. The use of targeting molecules on the MSN to improve nanoparticle specificity leads to a number of potential positive attributes. With improved accuracy, less material is needed, thus the exposure to the patient is reduced. Specificity also improves retention of therapeutics, which is important in the bladder where normal urination removes any soluble drugs. Here, a "fast on, slow off" approach is needed-the particles must selectively bind the tumor rapidly, and be able to interact with the target for an extended time. However, conferring specificity onto a nanoparticle comes with many challenges. Often, antibodies are used in pre-clinical trials which take advantage of cell surface markers that are overexpressed in cancer cells.[24, 36] These have resulted in little success and very little hope for the future clinical use, as most monoclonal antibodies are initially generated in rodents and thus are incompatible with human trials.

In this paper, we validate the MSN system within a pre-clinical model, first testing binding specificity *in vitro*, then subjecting the particles to the *in vivo* rigors of a bladder cancer animal model. Here, we will have the opportunity to test the contrast enhancement provided by the MSN *in vivo* using MRI and fluorescence/luminescence, and to compare *in vivo* specificity with our *in vitro* findings, as well as determine the retention of the particles within the bladder.

MATERIALS AND METHODS
Reagents
Dulbecco's modified eagle medium (DMEM), Roswell Park Memorial Institute (RPMI) 1640 medium, fetal bovine serum (FBS), penicillin-streptomycin (pen-strep), and Mem-PER™ Plus Membrane Protein Extraction Kit were purchased from Life Technologies (Grand Island, NY). Cetyltrimethylammonium bromide (CTAB, $CH_3(CH_2)_{15}N(CH_3)_3Br$), (3-aminopropyl)trimethoxysilane (APTMS) and tetraethoxysilane (TEOS) were purchased from Alfa Aesar (Ward Hill, MA). Fluorescein isothiocyanate (FITC) was purchased from Sigma-Aldrich (St. Louis, MO). Dimethyl sulfoxide (DMSO) was purchased from Fisher Scientific (Pittsburgh, PA). Protein assay dye reagent concentrate was purchased from Bio-Rad (Hercules, CA). Casein (Carnation® Instant Milk) was purchased from Nestle (Glendale, AZ). The Cyc6 peptide with a (gly-ser)[4] spacer (amino acid sequence SCVYAN-WRWTCGSGSGSGS) was synthesized by the Iowa State University Protein Core (Ames, IA).

Identification of a Bladder Cancer Specific Binding Peptide (BCSBP) Using Phage Display Libraries
The Cyc6 peptide was derived by previously described methods.[37] Briefly, a phage display library was generated

by digestion of 100 μg mJ$_1$ and synthesis of single-stranded oligonucleotide templates followed by double stranded DNA using Deep Vent polymerase and 10 cycles of primer extension PCR.[38] High affinity clones to be sequenced were grown as plaques on a lawn of DH5αF$'$ bacteria, then touched with a toothpick and suspended in 10 μL of 10 μM MgSO$_4$. This bacterial suspension was used as template for PCR. A total of 28 cycles of PCR were conducted and products were purified using a Qiaquick PCR purification kit (Qiagen, Valencia, CA). Five rounds of purification were carried out to increase enrichment (number of phages per bacterium) to 890, with saturation occurring after round 4.

Cell Culture/Labeling

Synthesis and characterization of MSN functionalized with gadolinium oxide and fluorescein isothiocyanate (Gd$_2$O$_3$-FITC-MSN) was obtained following previously reported syntheses.[25, 28, 39] Briefly, MSN were formed by addition of TEOS to CTAB, immediately followed by addition of Gd$_2$O$_3$ colloid. Next, FITC (5.0 mg, 0.0128 mmol) was reacted with APTMS (2.2345 μL, 0.0128 mmol) in DMSO for 2 hours, and TRITC-Gd$_2$O$_3$-MSN was prepared by grafting 0.05 mL of the resulting product on the previously synthesized Gd$_2$O$_3$-MSN. Particles were further functionalized by attachment of carbamic acid and EDC/NHS molecules,[40] used to attach the Cyc6 peptide, by resuspending a pellet of MSN in a supernatant containing the Cyc6 peptide at a weight ratio of 1.9 wt.% of the MSN weight and mixing overnight in a vortexer at low speed at 4 °C. The functionalization of MSN with Cyc6 was quantified by spectrophotometry (Nano-Drop 1000, Thermo Scientific, Waltham, MA), measuring the 280 nm absorbance of the supernatant before and after mixing.

Murine TCC cell line MB49[41] and human TCC cell line T24[42] are well-established; here, MB49 cells transfected with luciferase (luc) reporter genes, and normal T24 cells were cultured in RPMI 1640 medium supplemented with 10% FBS and pen-strep. A non-bladder cancer cell line, NIH3T3 mouse embryonic fibroblast,[43] was also prepared. Whole cells grown on poly-L-lysine-treated glass coverslips were exposed to Cyc6-Gd$_2$O$_3$-FITC-MSN at a concentration of 100 μg/mL for 4 hours, followed by rinsing of unbound particles. Fluorescent microscopy was used to visualize particle binding on whole cells, with acridine orange used as a nuclear stain.

To determine MSN-Cyc6 binding to an as-yet indeterminate target on the surface of MB49 cells, we carried out an extraction of all membrane proteins from the cell surface using the Mem-PER™ Plus Membrane Protein Extraction Kit. (Life Technologies, Grand Island, NY). Cells near confluence on tissue culture plastic were harvested for extraction of membrane proteins. A non-bladder cancer cell line, NIH3T3 mouse embryonic fibroblast,[43] was similarly prepared. The cells are permeabilized with a mild detergent to allow the release of soluble cytosolic proteins, then a second detergent solubilizes the membrane proteins. The concentration of the extraction is measured using a protein assay based on the principle of Bradford (Bio-Rad, Hercules, CA)[44] with known concentrations of bovine serum albumin used as standards. An acidic dye is added to protein solutions, and a color change occurring at 595 nm wavelength is measured on a microplate reader (SpectraMax, Molecular Devices, Sunnyvale, CA). Unknown concentrations are interpolated on a standard curve generated using known concentrations of bovine serum albumin. Based on total protein measurements, proteins were coated on a round bottom 96 well plate (0.1 mL @ 7 mg/mL) at 4 °C for 18 hours. To block non-specific binding, the membrane protein-coated wells were then exposed to casein (0.1 mL per well @ 50 μg/mL) for 1 hour at room temperature. The excess casein was removed and the membrane proteins were exposed to Gd$_2$O$_3$-FITC-MSN, Cyc6-Gd$_2$O$_3$-FITC-MSN, or Cyc6-Gd$_2$O$_3$-FITC-MSN pre-mixed for one hour with freely floating membrane proteins as a specific blocking agent (0.1 mL per well @ 2 mg/mL). The particles were allowed to bind for 90 minutes, at which point the plate was initially read in a fluorimetric plate reader (SpectraMax, Molecular Devices, Sunnyvale, CA) and washed. After each successive wash, the plate was read again, until the observed signal showed little change relative to the previous reading (a total of 3 washes). Each condition was carried out in triplicate, and Student's T-test was used for pairwise comparisons.

In Vivo Tumor Implantation

All procedures were performed according to NIH guidelines and previously approved by the Institutional Animal Care and Use Committee (IACUC). Tumor cells were instilled according to a well-established orthotopic model.[45] Female C57Bl/6 mice were anesthetized with a ketamine/xylazine mixture and the bladder was chemically burned by brief instillation of 5 μL 0.2 M silver nitrate, followed by rinsing with 100 μL phosphate buffered saline (PBS). A 50 μL suspension containing 5×10^5 MB49-Luc$^+$ cells in 50% normal mouse serum was instilled and retained in the bladder for one hour by catheter exclusion. After 6–8 days, tumor growth was verified by intraperitoneal injection of 0.1 mL luciferin at 15 mg/ml in PBS followed by *in vivo* luminescence imaging with the IVIS 200 system (Xenogen, Perkin-Elmer, Waltham, MA). Following confirmation of tumors in 3 mice, preliminary MRI scans were performed, then one mouse received an intravesicular instillation of Gd$_2$O$_3$-FITC-MSN without Cyc6 (1 mg MSN/50 μL PBS) and 2 mice received Cyc6-Gd$_2$O$_3$-FITC-MSN (1 mg MSN/50 μL PBS). Follow up MRI scans were acquired 24 hours after instillation of particles to allow for the elimination of free particles through urination.

Imaging/Image Processing

MRI scans were acquired using the Unity/INOVA 4.7 T small animal scanner (Varian, Palo Alto, CA) with a 25 mm gradient RF coil and fast spin echo multislice (fsems) sequences with T_1- or T_2-weighting (T_1-weighted scans: $T_R = 800$ ms, $T_E = 15$ ms, echo train length $= 8$, number of averages $= 10$; T_2-weighted scans: $T_R = 2000$ ms, $T_E = 15$ ms, echo train length $= 8$, number of averages $= 10$). Typical image dimensions are 512×512 with 30 slices and a voxel size of $0.068 \times 0.068 \times 0.4$ mm. The scanner produces raw DICOM image stacks that were converted to NIFTI format. Subsequent image processing used a custom MATLAB script that applies background removal[46] and reverse diffusion[47] algorithms to improve edge detection. The remainder of image processing and analysis was undertaken using the free medical imaging software MIPAV. Scans were normalized to one another by assigning a value of 1000 to the average intensity of fat adjacent to the kidneys, with all other values linearly interpolated between 0 and 1000. Volumes of interest (VOIs) were either manually drawn or semi-automatically selected using the "levelset VOI" tool in MIPAV. In addition, we measured urine intensity, prior and following injection of the particles and followed up over the duration of the experiment.

Statistical Analyses

Comparisons of measurements between groups of mice were made using Welch's method for the Student's T-test with populations of unequal variances: $t = (\bar{X}_1 - \bar{X}_2)/(\sqrt{(s_1^2/n_1) + (s_2^2/n_2)})$ with an alpha level of 0.05 considered significant. Significance was determined using degrees of freedom (d.f.) calculated by d.f. $= (s_1^2/n_1 + s_2^2/n_2)^2/((s_1^2/n_1)^2/(n_1 - 1) + (s_2^2/n_2)^2/(n_2 - 1))$. Comparisons of volumes within the same mouse were made using a two one-sided t-test (TOST)[48] with a significance level of $\alpha = 0.05$ and a test margin of 0.05 (a unitless value of normalized MRI intensity), representing the average smallest difference between two intensities that our image processing technicians could visually discern.

RESULTS/DISCUSSION

Particle Characterization and Peptide Attachment

Characterization of the core FITC-Gd_2O_3-MSN particle was reported previously. The samples used in this study were aliquots from a large synthesis described in greater detail in this previous study.[25] Characterization analytics are consistent throughout. Briefly, powder XRD analysis confirmed hexagonally arranged mesopores as evident by the intense d_{100}, and well resolved d_{110} and d_{200} peaks characteristic for MSN. Transmission electron micrographs of the Gd_2O_3-MSN particles showed this pattern as well as uniform size distributions and good dispersibility with little aggregation (Fig. 1(D), inset). The fully synthesized FITC-Gd_2O_3-MSN was characterized by

DLS; the median hydrodynamic diameter of the particles was 187.3 nm, with 96.3% of the particles falling within the primary distribution peak, spanning between 90 and 400 nm, resulting in a polydispersity index (PDI) of 0.535 (Fig. 1(B)). The concentration of Cyc6 peptide in the supernatant before and after mixing with MSN was measured spectroscopically by 280 nm absorbance (Fig. 1(E)). Direct measurement of the amount of peptide bound to the particles is hindered by the built-in fluorescence (FITC or TRITC) of the particles. Therefore, this value was derived from spectroscopic absorption at 280 nm. Initial peptide concentrations in the supernatant were compared with that after the admixture of the particles. Using this method, Cyc6 peptide binding to MSN is inferred using Beer's law, $A = e*L*C$, where A is the absorbance of 280 nm wavelength light, e is the extinction coefficient of the peptide (equal to 12,900 cm$^{-1} \cdot$ M^{-1} for the Cyc6 sequence and its spacer), L is the path length of the light (in cm) and c is the molar concentration of the peptide. Data shown (Fig. 1(E)) indicate at 280 nm absorbance the peptide was readily detected in the supernatant prior to mixing it with MSN, and nearly eliminated from the supernatant thereafter. The inherent imprecision in the calculation of extinction coefficient for peptides[49] implies that the values output by the device were taken as relative values. Thus, given a known initial concentration of 5 mM, the relative concentration of Cyc6 peptide in the supernatant after mixing with MSN particles was found to be 37.2% of the pre-mixing concentration. Hence the remaining 62.8%, or 3.14 mM, of the peptide in the pellet was considered linked to the particles. The total concentration of peptide bound to the particles was calculated to be 1.2 wt.% relative to the particles.

Cyc6-Functionalized MSN Particle Specificity for Bladder Cancer Cells

The bladder cancer cell specific peptide Cyc6 was identified using a phage display library with the filamentous bacteriophage M13 (Fig. 2). This peptide, and a heterocyclic variant HC1, were found to have nanomolar affinity for bladder cancer cells (Table II). Tested cells included normal mouse bladder (Fig. 2(A)), and two lines of mouse bladder cancer: MB49-1 (Fig. 2(B)), and MBT-2 (Fig. 2(C)). Mouse melanoma B16, human prostate cancer LNCaP, and human breast cancer MDA-MB453 were also negative for the protein (not shown).

In order to evaluate the specificity of Cyc6-functionalized MSN *in vitro*, binding was determined using fluorescent microscopy of whole cells and fluorimetric studies with extracted cell membrane proteins (Fig. 3). After 4 hours of binding, a clearly higher binding was observed on MB49 cells (Fig. 3(A)) than NIH3T3 cells (Fig. 3(B)). This was confirmed quantitatively on extracted membrane proteins (Fig. 3(C)), where relative fluorescein intensities indicated fluorescent Cyc6-functionalized MSN bound to MB49 proteins at a significantly higher rate than to NIH3T3 proteins ($p < 0.025$). In addition, the
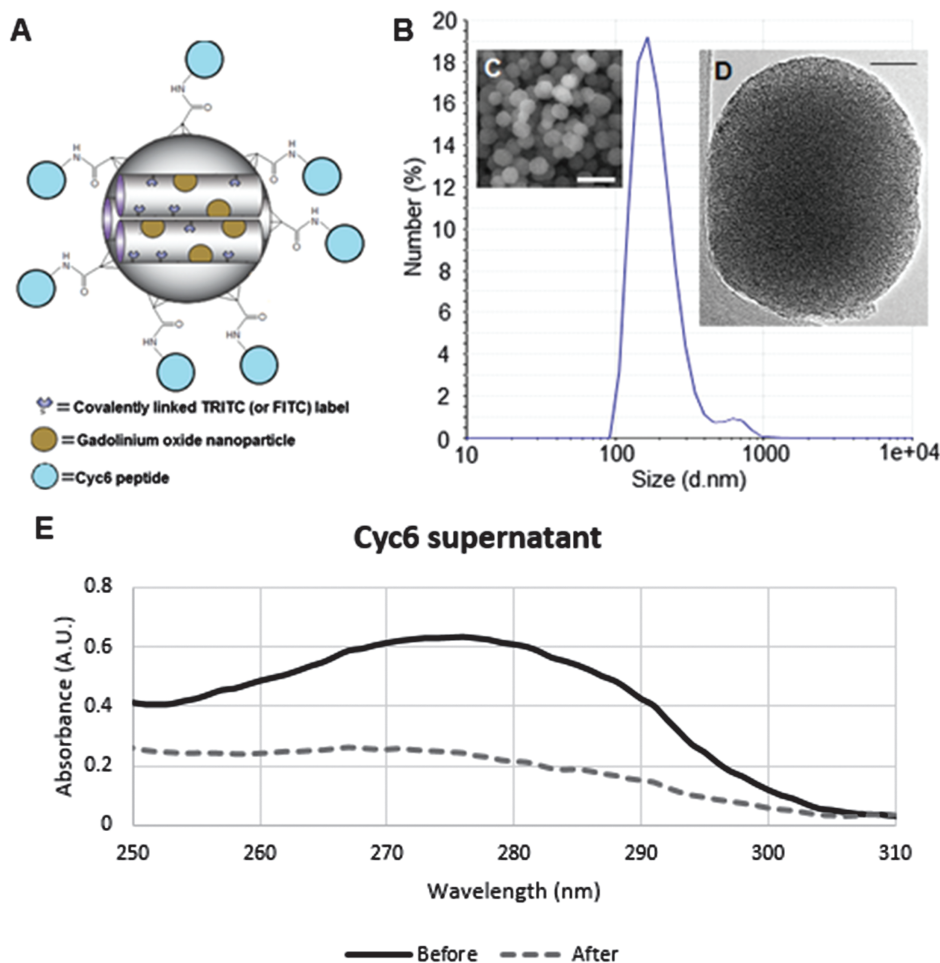
Figure 1. Characterization of mesoporous silica nanoparticles (MSN). (A) Schematic of MSN particle, functionalized with Cyc6 peptide and configured for fluorescent and MRI imaging. (B) Size distribution of PEG- and trifluoropropane-functionalized Gd_2O_3-TRITC-MSN, as measured by dynamic light scattering (DLS). The primary peak has a median particle size of 187.3 nm, and 96.3% of the particles are between 90 and 400 nm. The sample has a polydispersity index (PDI) of 0.535. (Inset (C)) Scanning electron micrograph (SEM) of several individual MSN particles, and transmission electron micrograph (TEM) of a single MSN (inset (D)). Estimated adsorption of targeting peptide Cyc6 (E). Quantitative evaluation of the adsorbed peptide was derived by calculating the concentration of remaining free peptide in the supernatant following exposure to the surface modified particles. Using Beer's law, the amount of bound peptide was computed to be 3.14 mM, or 1.2% by weight relative to the MSN particles in the sample. SEM scale bar, 500 nm; TEM scale bar, 50 nm.

Cyc6-functionalized membranes bound MB49 proteins at a higher rate than MSN without Cyc6, while the addition of freely floating MB49 membrane proteins further blocked binding.

Specificity of Cyc6 Peptide-Functionalized MSN in an Animal Bladder Cancer Model Measured by *In Vivo* MRI

In order to measure specificity of Cyc6 on bladder tumors *in vivo*, mouse bladder tumors were established followed by exposure to MSN with or without Cyc6 peptide. MRI scans acquired immediately prior to particle instillation were used as non-labeled controls. Follow-up MRI scans were performed 24 hours after particle instillation to ensure the clearance of unbound particles by urination. MRI evaluation of the urinary volume confirmed clearance: normalized T_1- and T_2-weighted MRI values were return to control levels (T_1: 398 ± 33; T_2: 664 ± 64) and MSN-exposed (T_1: 373 ± 21; T_2: 671 ± 194) bladders. Both values are indicative of insignificant particle concentrations remaining in the urine.

The segmented tumor volumes were measured in MRI to be 7.4, 9.5, and 15.9 mm³. The mouse with the 7.4 mm³ tumor received the FITC-Gd_2O_3-MSN instillation, and the other 2 mice received the Cyc6-FITC-Gd_2O_3-MSN. Follow-up MRI scans were acquired 24 hours after instillation (Fig. 4). MRI values were fat-normalized and plotted on the same color scale (Figs. 4(A–B)), with a clear hypointensity in the mice exposed to MSN functionalized with Cyc6. The average normalized value of
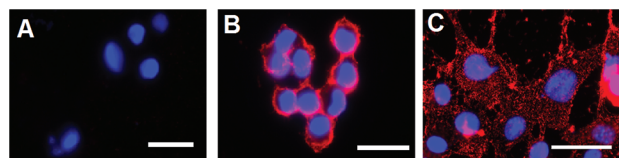
Figure 2. Immunological staining shows the specificity of the bladder cancer cell-derived sub-library. A bladder cancer specific cell surface peptide (BCSCSP) was identified using a phage display library with the filamentous bacteriophage M13 according to previously published methods.[37] Tested cells included normal mouse bladder (A), and two lines of mouse bladder cancer: MB49-1 (B), and MBT-2 (C). Each field is a composite of nuclear DNA staining with DAPI (blue) and immunofluorescent staining with an anti-M13 mouse monoclonal antibody and Cy3-conjugated secondary antibody (red). Scale bars indicate 20 μm.

the non-labeled tumors (582 ± 88) was reduced by FITC-Gd_2O_3-MSN (540 ± 118), and to a greater degree by Cyc6-FITC-Gd_2O_3-MSN (226 ± 34; $p < 0.0001$).

Identification of a Novel Bladder Cancer Cell Specific Peptide, Cyc6

Phage display is a method by which millions of different peptides can be screened at once against a target whose three dimensional structure is not known.[50, 51] Degenerate peptides are expressed as fusions to the coat protein pIII of bacteriophage M13 after ligation of a degenerate double stranded oligonucleotide into a phage display
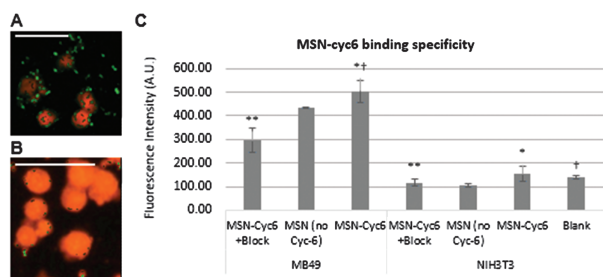

Figure 3. Mesoporous silica nanoparticles covalently linked with cyc6 peptide (MSN-cyc6) demonstrate higher affinity for MB49 cells than MSN alone. MB49 cells were grown on glass coverslips and exposed to MSN containing Gd_2O_3 and FITC, with (A) or without (B) cyc6, then washed (merge of red: nuclei stained with acridine orange; and green: particles containing FITC). Clusters of MSN-cyc6 particles can be seen closely associated with MB49 cells, whereas MSN particles without cyc6 are considerably sparser. (C) Membrane proteins were isolated from MB49 bladder cancer and NIH3T3 fibroblast cell lines, plated, and exposed to MSN containing Gd_2O_3 and FITC, with or without cyc6 and with or without casein to block non-specific binding (blocking solution: 5% milk powder in PBS). After washing away unbound particles, the FITC fluorescence intensity was measured. The addition of cyc6 to the MSN increases the level of binding by 16% over MSN without cyc6, and by 70% over casein-blocked membranes. Error bars indicate standard deviation (*—$p < 0.025$; **—$p < 0.05$; †—$p < 0.0001$ for pairwise comparisons between data with matching symbols). Scale bar = 10 μm.
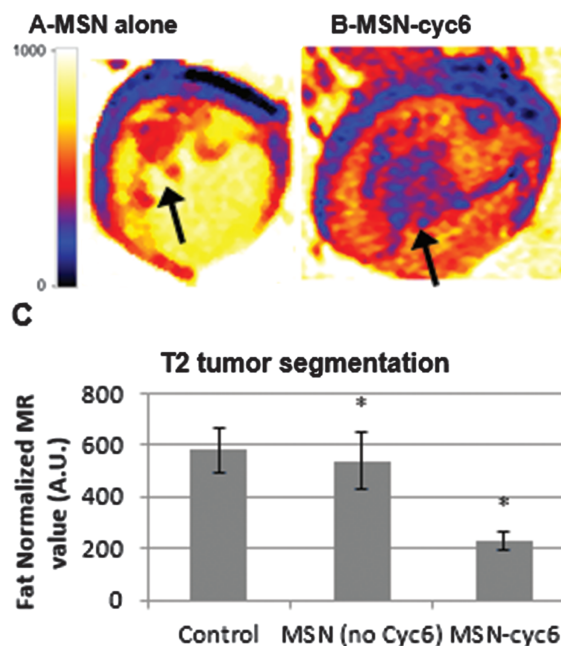
Figure 4. MSN conjugated to cyc6 peptide has a higher affinity for bladder cancer than MSN alone. Fat-normalized pseudocolor slices of *in vivo* T_2-weighted MRI of bladder tumors (arrows), labeled with MSN alone (no cyc6, (A)), and MSN conjugated to cyc6 (B), with hypointensity (darker color) indicative of increased binding of MSN. (C) The mean normalized T_2-weighted MRI values for control (unlabeled) bladder tumors prior to labeling, and tumors labeled with MSN and MSN-cyc6. The greater hypointensity for the tumor labeled with MSN-cyc6 indicates more particle binding than MSN alone. Error bars indicate standard deviation of tumor intensity (*—$p < 0.0001$ for pairwise comparisons between data with matching symbols).

vector. The phage library is then incubated with a target (i.e., a bladder cancer cell), washed extensively, eluted and, if needed, amplified. After several rounds of affinity purification, individual phage clones are plaque-purified and screened. The best phage clones can be further amplified in bacteria, isolated as double stranded DNA (replicative form), and subjected to DNA sequencing to determine the sequence of the expressed peptide.

We, with the collaborating laboratory of Dr. John V. Frangioni, have constructed a novel type 3 phage display vector with several properties that optimize expression of peptides as pIII fusions (vector mJ_1). Using mJ_1, we have constructed three highly degenerate eight amino acid libraries in three different structures:

(1) linear (L8 library),
(2) cyclic via flanking cysteine residues that auto-oxidize in the bacterial periplasm (C8 library; ten amino acids total, including flanking cysteine residues), and
(3) heterocyclic with four degenerate linear amino acids followed by four cysteine-cyclized amino acids (L4C4 library; ten amino acids total, including flanking cysteine residues, Table I).

237

Table I. Amino acid sequences of bladder cancer-specific binding peptides (BCSBPs).

Structure	Clone #	Peptide sequence
Heterocyclic	**1**, 2, 8, 9 10, 11, 14, 16, 17, 18	S I S L G C W G P F C (GS)4
	3	S V S L G C F G P W C (GS)4
	4, 19	S I G L G C W G P F C (GS)4
	5	S V S L G C W G L F C (GS)4
	7	S V S L N C W G I A C (GS)4
	12, 20	S M S L G C W G P W C (GS)4
	13	S I S L G C F G R F C (GS)4
	Consensus	α S L G C W G P ϕ C
Cyclic	**6**	S C V Y A N W R W T C (GS)4
	15	S C V Y S N W R W Q C (GS)4
	Consensus	C V Y x N W R W x C

Notes: α = aliphatic residues, ϕ = Phe or Trp, x = any amino acid.

Each peptide is 1,100 M.W. or less prior to addition of the (gly-ser) spacer. A length of eight degenerate positions was chosen to balance size minimization, diversity, helix formation (two and one half turns for linear peptides) and ring constraint (for cyclic and heterocyclic peptides). Sequencing of random clones from the libraries has confirmed the expected representation of all amino acids, except for a slight enrichment for tryptophan (data not shown). We routinely use an equi-complex mixture of all three libraries for screening since one or more structures may be preferentially selected by the target. Using living MB49 cells as the target for phage affinity purification, an equi-complex mixture of the three phage display libraries was purified for five rounds. There was a successive enrichment of phage binding to these cells, with saturation occurring after round 4 of affinity purification. Correlating with enrichment was a strong signal as assayed by indirect immunofluorescence.

Twenty individual phage clones were then plaque-purified and subjected to DNA sequence analysis. Of the 20 clones, 18 had an identical peptide sequence, or varied by only a single amino acid (Table I). The remaining 2 clones differed from each other by only a single amino acid, but had a completely different sequence (and peptide structure) when compared to the other 18 peptides. Hence, two families of bladder cancer binding peptides were discovered. Two (heterocyclic clone number 1 and cyclic clone number 6) had the highest affinity and are shown herein (Table II). The actual per peptide affinity of these bladder cancer-derived peptides must await cloning of the as yet unknown cell surface target(s); however, based on

Table II. Properties of bladder cancer-specific binding peptides (BCSBPs).

Name	Structure	Clone #	Binding affinity (nM)	Mol. Wt. (Da)	Ext. Coef. (cm^{-1} · M^{-1})
HC1	Heterocyclic	1	10–50	1746	5930
Cyc6	Cyclic	6	10–50	1965	12900

comparisons to other phage/target model systems, actual affinity is likely in the 10–50 nM range. Indeed, phage binding to the surface of MB49 after 4 rounds of affinity purification cells is intense (Fig. 2) with only high pico-molar to low nanomolar concentrations of applied phage. Most importantly, phage derived from MB49 bladder cancer cells appear quite specific for bladder cancer in general. These phage (and hence peptides) also bind to the unrelated mouse bladder cancer cell line MBT-2 (Fig. 2).[52] MB49 derived phage also bind equally well to six of six human bladder cancer cell lines tested, a resected low-grade human surgical specimen (data not shown), and a canine bladder cancer cell line K9-TCC (data not shown). Hence, the antigen recognized by these peptides is likely homologous in mouse, human and dog, is highly expressed on the cell surface, and may play an essential role in pathogenesis of the disease.

Cyc6-Functionalized MSN Show Enhanced Specificity for Bladder Cancer Cells and Extracted Membrane Proteins *In Vitro*

Once identified, the 11 peptide sequence for Cyc6 was synthesized including a 4× repeat of (glycine-serine) onto the *C*-terminus. The FITC-Gd$_2$O$_3$-MSN particles were further functionalized with EDC/NHS molecules via a carbamic acid linker.[40] Binding to EDC/NHS occurs by way of a primary amine, though the exact amine by which the Cyc6 peptide binds to the MSN is unknown. The synthesized peptide has 3 primary amines: the *N*-terminus, the arginine residue, and the asparagine residue. In future studies to further characterize the Cyc6-MSN binding, the (glycine-serine) spacer may be substituted for other residues as needed while keeping the primary peptide sequence unchanged. The EDC/NHS technique allows for peptide binding by simple stirring. Thus, a pellet of FITC-Gd$_2$O$_3$-MSN was resuspended in a supernatant containing the Cyc6 peptide and mixed on a vortexer at low speed overnight at 4 °C. After mixing, the particles were centrifuged at 16,000 × g for 10 minutes, and 10 μL supernatant samples from before and after mixing were measured on a Nano-Drop 1000 UV-Vis spectrophotometer as described above.

Given sufficient time (up to 24 hours), we have observed near-total binding of non-specific FITC-Gd$_2$O$_3$-MSN on MB49 mouse TCC cells. However in clinical settings, there is a need for more rapid binding of bladder cancer cells and longer retention of bound particles (a "fast on, slow off" approach). In order to test the enhancement of rapid binding by Cyc6-FITC-Gd$_2$O$_3$-MSN to MB49 cells, binding was carried out for a maximum of 4 hours in tissue culture, at which point unbound particles were rinsed from the cells with phosphate buffered saline. Given a shorter window for binding, a high level of binding was observed under fluorescent microscopy for Cyc6-functionalized MSN on MB49 cells (Fig. 3(A)) compared

with almost no binding for non-functionalized MSN. Thus we observe a higher affinity of our MSN for bladder cancer cells when functionalized with Cyc6.

The specificity was evaluated using an *in vitro* binding assay, in which extracted membrane proteins from MB49 cells were compared with those of NIH3T3, a non-bladder cancer murine cell line. In preliminary experiments, the membrane protein concentration was varied between 0–7 mg/mL, and the MSN concentration was varied between 0–3 mg/mL. We concluded that 7 mg/mL of membrane protein was sufficient to have a contiguous coat of protein on the surface of the well, preventing non-specific binding of MSN at 2 mg/mL to the plastic. The particles were allowed to bind for 90 minutes, at which point the plate was successively read and washed for 3 washes. Results (Fig. 3(C)) show demonstrably higher retention of all types of particles in MB49 cells relative to NIH3T3 cells, which show an equivalent level of retention of fluorescence to an untreated (blank) well into which Cyc6-FITC-Gd$_2$O$_3$-MSN were added. The functionalized Cyc6-FITC-Gd$_2$O$_3$-MSN show a statistically significantly higher binding to MB49 than to NIH3T3 ($p < 0.025$). It also showed a slightly increased binding to MB49 relative to non-functionalized FITC-Gd$_2$O$_3$-MSN, and in addition, the use of free MB49 membrane proteins as a blocking agent further reduced binding, though these differences were not statistically significant (p-values of 0.14 and 0.18, respectively).

Taken in total, the data (Figs. 2, 3) indicate the Cyc6-FITC-Gd$_2$O$_3$-MSN do show improved specificity *in vitro*, both in terms of more rapid binding to MB49 cells relative to non-functionalized FITC-Gd$_2$O$_3$-MSN, and higher binding in MB49 cells relative to non-bladder cancer cells. As stated above, the target of the peptide on the bladder cancer cell has not been identified, nor has the site on which the peptide binds to the MSN. In future work, the former may be addressed by a combination of molecular biology and informatics techniques, while the latter may be determined by synthesizing new peptides with small sequence changes that affect the location of primary amines. By characterizing these properties we may be able to further enhance binding specificity as needed, resulting in additional improvements to *in vivo* bladder cancer labeling.

Cyc6-Functionalized MSN Show Enhanced Specificity for Bladder Tumors in a Mouse *In Vivo* Model

In pre-clinical and clinical MRI, images are frequently acquired with T_1- or T_2-weighting, with T_1 referring to the spin-lattice, or flip angle, relaxation time, and T_2 referring to the spin-spin, or precessional relaxation time. Weighting is controlled by the MRI operator typically by varying the echo time (T_E) or relaxation time (T_R); T_1-weighted scans typically have a short T_R and T_E, while T_2-weighted scans have a longer T_R and T_E. A third imaging strategy using long T_R and short T_E minimizes T_1 and T_2 effects

to generate an image based more on proton density.[53] On our Varian® 4.7 T small animal scanner, we have optimized scan parameters for proton density with slight T_1- and T_2-weighting; a typical T_1 weighted scan has a T_R of 800 ms and a T_E of 15 ms, while a typical T_2-weighted scan has a T_R of 2300 ms and a T_E of 15 ms. Using these parameters, the T_2-weighted scan typically provides better anatomical details, while both T_1- and T_2-weighted scans are enhanced by Gd$_2$O$_3$ contrast agents. These agents have moderate relaxivity values for both R_1 and R_2 and thus can provide contrast in T_1- and T_2-weighted MRI.[29, 54] Thus, data presented herein emphasize T_1-weighting when more quantitative contrast is shown, and T_2-weighting when qualitative anatomic changes are shown. Study controls include no treatment (a negative control) as well as MSN without Cyc6. However, no gold standards used clinically can serve as a suitably comparable gold standard in our experimental paradigm. ImmunoCyt/uCyt™ and UroVysion™ are *ex vivo* tests which use monoclonal antibodies and *in situ* hybridization probes, respectively, on biopsied tissues[55, 56] rather than an *in vivo* imaging approach. Hexvix, or hexyl aminolevulinate, is a dye containing porphyrins used in conjunction with fluorescent cystoscopy.[12] Cancer cells absorb the dye more readily than healthy epithelium and fluoresce pink. To date, we have not seen a report of cystoscopy-based approaches in murine models.

Unlike CT, PET, and ultrasound, in which the image output is directly related to a physical property (density, positron emission, and acoustic impedance, respectively), the output of an MRI scan is unitless, with relative grayscale values related to the frequency response of the tissue to a particular pulse sequence. Thus, it is important to implement a consistent normalization strategy for comparison of tissues between different subjects and scans. To date, there is no agreed-upon methodology for normalizing MRI scans, though it is important that the normalization is consistent, replicable, and robust.[57] Thus, we have implemented a normalization strategy that involves calculating the mean grayscale value of a region of fat, setting it to an arbitrary value such as 100 or 1000, and interpolating all values in the image between 0 and the arbitrary value. Fat is an ideal candidate for normalization because it is homogeneous, nearly always the brightest tissue in the scan, and with minimal vascularity, unlikely to be acutely affected by the intravenous or intravesicular injection of contrast agents.

Initially, 6 mice received intravesicular transplants of MB49 murine TCC cells. One week after implantation, 3 mice were determined by luciferase activity to have consistent tumor sizes and were justifiable for comparison. One other mouse had a very large tumor, and 2 others had almost no tumor. Immediately following the first set of IVIS scans, the 3 mice were taken to the small animal MRI; acquisitions include T_1-weighted axial scans, T_2-weighted axial scans, and T_1-weighted

coronal scans. The mice were then given intravesicular instillation of 50 μL injections containing either FITC-Gd_2O_3-MSN or Cyc6-FITC-Gd_2O_3-MSN, and re-scanned the following day. The T_1- and T_2-weighted axial scans were fat-normalized, and representative T_2-weighted slices from each bladder are shown (Fig. 4). With T_1-weighting, the borders of the tumors were difficult to identify, but appear as a slight lightening of the surrounding bladder space. The tumors are also slightly lighter than the bladder wall. With T_2-weighting, the tumor boundaries are much more distinct; the tumors show up as hypointense relative to the bladder space. Although the tumor boundaries were less clearly defined in the T_1-weighted MRI than the T_2 scans, the tumor volumes measured in each were consistent for all 3 mice, corroborating the IVIS findings.

The normalized T_1 intensities observed for the Cyc6-FITC-Gd_2O_3-MSN-exposed mice were higher than that of the FITC-Gd_2O_3-MSN-exposed mouse, while the T_2-weighted intensities for the Cyc6-FITC-Gd_2O_3-MSN-exposed mice were significantly more hypointense than that of the FITC-Gd_2O_3-MSN-exposed mouse. Taken together, this data indicates that the MSN containing Cyc6 have bound more effectively to the tumor than MSN alone. In this mouse model, the mice are typically sacrificed 2–3 weeks following the initial transplantation of the tumor. When the bladder is excised and sectioned, we observe fluorescence in the tumor, indicating strong retention of the particles. In addition, the mice were tested for a systemic immune response based on interferon-gamma (IFN-γ) production by splenocytes when stimulated with Cyc6. No IFN-γ production was detected. Because instillation was performed directly in the bladder, secondary organs (liver and kidneys) were not exposed to particles in this study. However, additional studies of intravenously injected MSN show no histopathological evidence of co-morbidity in exposed mice. Briefly, a number of cell lines were viable following doses up to 125 μg/mL in culture, and mice tolerated exposures up to 1 mg delivered intravenously (by tail vein or retro-orbital injection) without adverse changes in inflammatory cytokine production. In pregnant mice, we saw no evidence of adverse immune reaction or impact on growth in length or weight of the mothers or the embryos.

CONCLUSIONS

The data presented herein support our prediction that, with improved specificity via a molecular target on bladder cancer cells, we improved affinity of our particles for bladder cancer cells both *in vitro* and *in vivo*. This finding ultimately has many valuable clinical implications. Gadolinium oxide contrast agents functionalized with the bladder cancer cell specific peptide Cyc6 are shown to enhance MRI contrast and bind preferentially to bladder cancer cells relative to normal bladder epithelium. Thus, in a clinical setting, a scenario in which particles are instilled in

the bladder, and within 4 hours, visualized by fluorescent cystoscopy or using T_1- and T_2-weighted MRI, is feasible. Unlike many pre-clinical targeting approaches which use monoclonal antibodies,[58, 59] the Cyc6 peptide is small and non-immunogenic, with the potential to be readily translated from pre-clinical to clinical medicine. Finally, an advantage of MSN materials is their capacity for loading and release of reagents from the porous cores. Studies are ongoing to load and deliver anti-cancer reagents directly to the bladder using a targeted approach. Thus, this technology has the potential to improve both the diagnostic and therapeutic approach to bladder cancer.

Conflict of Interest

Jose G. Assouline is founder and sole proprietor of NanoMedTrix, LLC, which prepared the nanoparticles used in this study. All results and claims have been independently verified by other scientists with no financial stake in the company.

REFERENCES

1. R. L. Siegel, K. D. Miller, and A. Jemal, Cancer statistics. *CA Cancer. J. Clin.* 65, 5 (**2015**).
2. E. B. Avritscher, C. D. Cooksley, H. B. Grossman, A. L. Sabichi, L. Hamblin, C. P. Dinney, and L. S. Elting, Clinical model of lifetime cost of treating bladder cancer and associated complications. *Urology* 68, 549 (**2006**).
3. D. L. Lamm, B. A. Blumenstein, E. D. Crawford, J. E. Montie, P. Scardino, H. B. Grossman, T. H. Stanisic, J. A. Smith, Jr., J. Sullivan, and M. F. Sarosdy, A randomized trial of intravesical doxorubicin and immunotherapy with bacille calmette-guerin for transitional-cell carcinoma of the bladder. *N. Engl. J. Med.* 325, 1205 (**1991**).
4. T. J. Kemp, A. T. Ludwig, J. K. Earel, J. M. Moore, R. L. Vanoosten, B. Moses, K. Leidal, W. M. Nauseef, and T. S. Griffith, Neutrophil stimulation with mycobacterium bovis bacillus calmette-guerin (BCG) results in the release of functional soluble TRAIL/Apo-2L. *Blood* 106, 3474 (**2005**).
5. M. C. Hall, S. S. Chang, G. Dalbagni, R. S. Pruthi, J. D. Seigne, E. C. Skinner, J. S. Wolf, Jr., and P. F. Schellhammer, Guideline for the management of nonmuscle invasive bladder cancer (stages Ta, T_1, and Tis): 2007 update. *J. Urol.* 178, 2314 (**2007**).
6. D. S. Kaufman, W. U. Shipley, and A. S. Feldman, Bladder cancer. *Lancet.* 374, 239 (**2009**).

7. O. R. Faba, J. Palou, A. Breda, and H. Villavicencio, High-risk non-muscle-invasive bladder cancer: Update for a better identification and treatment. *World J. Urol.* 30, 833 (**2012**).

8. V. H. Nargund, C. K. Tanabalan, and M. N. Kabir, Management of non-muscle-invasive (superficial) bladder cancer. *Semin. Oncol.* 39, 559 (**2012**).

9. J. J. Liu, M. J. Droller, and J. C. Liao, New optical imaging technologies for bladder cancer: Considerations and perspectives. *J. Urol.* 188, 361 (**2012**).

10. T. Filbeck, U. Pichlmeier, R. Knuechel, W. F. Wieland, and W. Roessler, Do patients profit from 5-aminolevulinic acid-induced fluorescence diagnosis in transurethral resection of bladder carcinoma. *Urology* 60, 1025 (**2002**).

11. F. N. Joudi and B. R. Konety, Fluorescence cystoscopy and bladder surveillance. *Curr. Opin. Urol.* 14, 265 (**2004**).

12. C. Martoccia, M. Zellweger, B. Lovisa, P. Jichlinski, H. van den Bergh, and G. Wagnieres, Optical spectroscopy of the bladder washout fluid to optimize fluorescence cystoscopy with hexvix(R). *J. Biomed. Opt.* 19, 97002 (**2014**).

13. D. Zaak, A. Karl, R. Knuchel, H. Stepp, A. Hartmann, O. Reich, A. Bachmann, M. Siebels, G. Popken, and C. Stief, Diagnosis of urothelial carcinoma of the bladder using fluorescence endoscopy. *BJU Int.* 96, 217 (**2005**).

14. H. B. Grossman, M. Soloway, E. Messing, G. Katz, B. Stein, V. Kassabian, and Y. Shen, Surveillance for recurrent bladder cancer using a point-of-care proteomic assay. *JAMA* 295, 299 (**2006**).

15. L. Cheng, R. Montironi, D. D. Davidson, and A. Lopez-Beltran, Staging and reporting of urothelial carcinoma of the urinary bladder. *Mod. Pathol.* 22 (Suppl 2), S70 (**2009**).

16. A. P. Mitra, M. Jorda, and R. J. Cote, Pathological possibilities and pitfalls in detecting aggressive bladder cancer. *Curr. Opin. Urol.* 22, 397 (**2012**).

17. D. L. Lamm, B. A. Blumenstein, J. D. Crissman, J. E. Montie, J. E. Gottesman, B. A. Lowe, M. F. Sarosdy, R. D. Bohl, H. B. Grossman, T. M. Beck, J. T. Leimert, and E. D. Crawford, Maintenance bacillus calmette-guerin immunotherapy for recurrent TA, T_1 and carcinoma *in situ* transitional cell carcinoma of the bladder: A randomized southwest oncology group study. *J. Urol.* 163, 1124 (**2000**).

18. M. Brausi, J. Oddens, R. Sylvester, A. Bono, C. van de Beek, G. van Andel, P. Gontero, L. Turkeri, S. Marreaud, S. Collette, and W. Oosterlinck, Side effects of bacillus calmette-guerin (BCG) in the treatment of intermediate- and high-risk Ta, T_1 papillary carcinoma of the bladder: Results of the EORTC genito-urinary cancers group randomised phase 3 study comparing one-third dose with full dose and 1 year with 3 years of maintenance BCG. *Eur. Urol.* 65, 69 (**2014**).

19. T. Ochiai, H. Sato, R. Hayashi, T. Asano, H. Sato, and Y. Yamamura, Postoperative adjuvant immunotherapy of gastric cancer with BCG-cell wall skeleton, 3- to 6-year follow up of a randomized clinical trial. *Cancer Immunol. Immunother.* 14, 167 (**1983**).

20. D. Connolly, S. Currivan, and B. Paull, Polymeric monolithic materials modified with nanoparticles for separation and detection of biomolecules: A review. *Proteomics* 12, 2904 (**2012**).

21. C. Huang, K. G. Neoh, L. Xu, E. T. Kang, and E. Chiong, Polymeric nanoparticles with encapsulated superparamagnetic iron oxide and conjugated cisplatin for potential bladder cancer therapy. *Biomacromolecules* 13, 2513 (**2012**).

22. T. Nakamura, M. Fukiage, M. Higuchi, A. Nakaya, I. Yano, J. Miyazaki, H. Nishiyama, H. Akaza, T. Ito, H. Hosokawa, T. Nakayama, and H. Harashima, Nanoparticulation of BCG-CWS for application to bladder cancer therapy. *J. Control. Release* 176, 44 (**2014**).

23. S. Z. Nergiz, N. Gandra, S. Tadepalli, and S. Singamaneni, Multifunctional hybrid nanopatches of graphene oxide and gold nanostars for ultraefficient photothermal cancer therapy. *ACS Appl. Mater. Interfaces* 6, 16395 (**2014**).

24. C. H. Chen, Y. J. Wu, and J. J. Chen, Gold nanotheranostics: Photothermal therapy and imaging of mucin 7 conjugated antibody nanoparticles for urothelial cancer. *Biomed. Res. Int.* 2015, 813632 (**2015**).

25. S. K. Sweeney, Y. Luo, M. A. O'donnell, and J. G. Assouline, Nanotechnology and cancer: Improving real-time monitoring and staging of bladder cancer with multimodal mesoporous silica nanoparticles. *Cancer Nanotechnology* 7, 3 (**2016**).

26. T. Liu, L. Li, X. Teng, X. Huang, H. Liu, D. Chen, J. Ren, J. He, and F. Tang, Single and repeated dose toxicity of mesoporous hollow silica nanoparticles in intravenously exposed mice. *Biomaterials* 32, 1657 (**2011**).

27. J. Duan, Y. Yu, Y. Li, Y. Yu, Y. Li, X. Zhou, P. Huang, and Z. Sun, Toxic effect of silica nanoparticles on endothelial cells through DNA damage response via Chk1-dependent G2/M checkpoint. *PLoS One* 8, e62087 (**2013**).

28. J. L. Bridot, A. C. Faure, S. Laurent, C. Riviere, C. Billotey, B. Hiba, M. Janier, V. Josserand, J. L. Coll, L. V. Elst, R. Muller, S. Roux, P. Perriat, and O. Tillement, Hybrid gadolinium oxide nanoparticles: Multimodal contrast agents for *in vivo* imaging. *J. Am. Chem. Soc.* 129, 5076 (**2007**).

29. J. Y. Park, M. J. Baek, E. S. Choi, S. Woo, J. H. Kim, T. J. Kim, J. C. Jung, K. S. Chae, Y. Chang, and G. H. Lee, Paramagnetic ultrasmall gadolinium oxide nanoparticles as advanced T_1 MRI contrast agent: Account for large longitudinal relaxivity, optimal particle diameter, and *in vivo* T_1 MR images. *ACS Nano* 3, 3663 (**2009**).

30. M. B. Myers, Prediction of skin sloughs at the time of operation with the use of fluorescein dye. *Surgery* 51, 158 (**1962**).

31. P. J. Doyle, L. Lipetskaia, E. Duecy, G. Buchsbaum, and R. W. Wood, Sodium fluorescein use during intraoperative cystoscopy. *Obstet. Gynecol.* 125, 548 (**2015**).

32. V. Vejzovic, A. Wennick, E. Idvall, D. Agardh, and A. C. Bramhagen, Polyethylene glycol or sodium picosulphate based laxatives prior to colonoscopy in children: Randomized controlled trial. *J. Pediatr. Gastroenterol. Nutr.* 62, 414 (**2015**).

33. K. Kurth, W. J. Vijgh, F. ten Kate, J. F. Bogdanowicz, P. J. Carpentier and I. Van Reyswoud, Phase 1/2 study of intravesical epirubicin in patients with carcinoma *in situ* of the bladder. *J. Urol.* 146, 1508, discussion 1512 (**1991**).

34. T. Tsushima, Y. Miyaji, M. Noda, Y. Nasu, H. Kumon, and H. Ohmori, Absorption of epirubicin instilled intravesically immediately after transurethral resection of superficial bladder cancer. *Urol. Int.* 60, 161 (**1998**).

35. Y. Yamamoto, Y. Nasu, T. Saika, T. Akaeda, T. Tsushima, and H. Kumon, The absorption of pirarubicin instilled intravesically immediately after transurethral resection of superficial bladder cancer. *BJU Int.* 86, 802 (**2000**).

36. F. Y. Cheng, C. T. Chen, and C. S. Yeh, Comparative efficiencies of photothermal destruction of malignant cells using antibody-coated silica@Au nanoshells, hollow Au/Ag nanospheres and Au nanorods. *Nanotechnology* 20, 425104-4484/20/42/425104 (**2009**).

37. S. D. Voss, A. M. DeGrand, G. R. Romeo, L. C. Cantley, and J. V. Frangioni, An integrated vector system for cellular studies of phage display-derived peptides. *Anal. Biochem.* 308, 364 (**2002**).

38. B. K. Kay, J. Winter, and J. McCafferty, Phage Display of Peptides and Proteins: A Laboratory Manual, Academic Press, San Diego (**1996**).

39. Y. S. Lin, N. Abadeer, K. R. Hurley, and C. L. Haynes, Ultrastable, redispersible, small, and highly organomodified mesoporous silica nanotherapeutics. *J. Am. Chem. Soc.* 133, 20444 (**2011**).

40. G. T. Hermanson, Bioconjugate Techniques, 2nd edn., Elsevier Academic Press, Burlington, MA (**2008**).

41. I. C. Summerhayes and L. M. Franks, Effects of donor age on neoplastic transformation of adult mouse bladder epithelium *in vitro*. *J. Natl. Cancer Inst.* 62, 1017 (**1979**).

42. J. Bubenik, M. Baresova, V. Viklicky, J. Jakoubkova, H. Sainerova, and J. Donner, Established cell line of urinary bladder carcinoma

(T24) containing tumour-specific antigen. *Int. J. Cancer* 11, 765 (**1973**).

43. K. A. Westerman and P. Leboulch, Reversible immortalization of mammalian cells mediated by retroviral transfer and site-specific recombination. *Proc. Natl. Acad. Sci. U.S.A.* 93, 8971 (**1996**).

44. M. M. Bradford, A rapid and sensitive method for the quantitation of microgram quantities of protein utilizing the principle of protein-dye binding. *Anal. Biochem.* 72, 248 (**1976**).

45. Y. Luo, X. Chen, and M. A. O'donnell, Use of prostate specific antigen to measure bladder tumor growth in a mouse orthotopic model. *J. Urol.* 172, 2414 (**2004**).

46. O. Salvado, C. Hillenbrand, S. Zhang, and D. L. Wilson, Method to correct intensity inhomogeneity in MR images for atherosclerosis characterization. *IEEE Trans. Med. Imaging* 25, 539 (**2006**).

47. O. Salvado, C. M. Hillenbrand, and D. L. Wilson, Partial volume reduction by interpolation with reverse diffusion. *Int. J. Biomed. Imaging* 2006, 92092 (**2006**).

48. C. W. Hong, S. Rais-Bahrami, A. Walton-Diaz, N. Shakir, D. Su, A. K. George, M. J. Merino, B. Turkbey, P. L. Choyke, B. J. Wood, and P. A. Pinto, Comparison of magnetic resonance imaging and ultrasound (MRI-US) fusion-guided prostate biopsies obtained from axial and sagittal approaches. *BJU Int.* 115, 772 (**2015**).

49. S. C. Gill and P. H. von Hippel, Calculation of protein extinction coefficients from amino acid sequence data. *Anal. Biochem.* 182, 319 (**1989**).

50. S. M. Lee, E. J. Lee, H. Y. Hong, M. K. Kwon, T. H. Kwon, J. Y. Choi, R. W. Park, T. G. Kwon, E. S. Yoo, G. S. Yoon, I. S. Kim, E. Ruoslahti, and B. H. Lee, Targeting bladder tumor cells *in vivo* and in the urine with a peptide identified by phage display. *Mol. Cancer Res.* 5, 11 (**2007**).

51. L. Seung-Min, Y. Gil-Suk, Y. Eun-Sang, K. Tae-Gyun, K. In-San, and L. Byung-Heon, Application of phage display to discovery of tumor-specific homing peptides: Developing strategies for therapy

and molecular imaging of cancer. *Methods Mol. Biol.* 512, 355 (**2009**).

52. M. S. Soloway, Intravesical and systemic chemotherapy of murine bladder cancer. *Cancer Res.* 37, 2918 (**1977**).

53. Z. Liang and P. C. Lauterbur, IEEE engineering in medicine and biology society, Principles of Magnetic Resonance Imaging: A Signal Processing Perspective, SPIE Optical Engineering Press, Bellingham, Wash, New York (**2000**).

54. M. J. Lee, M. J. Kim, C. S. Yoon, S. Y. Song, K. Park, and W. S. Kim, The T_2-shortening effect of gadolinium and the optimal conditions for maximizing the CNR for evaluating the biliary system: A phantom study. *Korean J. Radiol.* 12, 358 (**2011**).

55. M. E. Vergara-Lluri, E. Hu, J. Y. Rao, M. Levin, S. K. Apple, and N. A. Moatamed, Comparative evaluation of ProEx C and Immuno-Cyt/uCyt assays in atypical urine cytology. *Arch. Pathol. Lab. Med.* 138, 1215 (**2014**).

56. C. Seideman, D. Canter, P. Kim, B. Cordon, A. Weizer, I. Oliva, J. Rao, B. A. Inman, M. Posch, H. Herr, and Y. Lotan, Multicenter evaluation of the role of UroVysion FISH assay in surveillance of patients with bladder cancer: Does FISH positivity anticipate recurrence?. *World J. Urol.* 33, 1309 (**2015**).

57. R. T. Shinohara, E. M. Sweeney, J. Goldsmith, N. Shiee, F. J. Mateen, P. A. Calabresi, S. Jarso, D. L. Pham, D. S. Reich, and C. M. Crainiceanu, Australian imaging biomarkers lifestyle flagship study of ageing and alzheimer's disease neuroimaging initiative, statistical normalization techniques for magnetic resonance imaging. *Neuroimage Clin.* 6, 9 (**2014**).

58. D. Artemov, Molecular magnetic resonance imaging with targeted contrast agents. *J. Cell Biochem.* 90, 518 (**2003**).

59. J. Qiao, S. Li, L. Wei, J. Jiang, R. Long, H. Mao, L. Wei, L. Wang, H. Yang, H. E. Grossniklaus, Z. R. Liu, and J. J. Yang, HER2 targeted molecular MR imaging using a de novo designed protein contrast agent. *PLoS One* 6, e18103 (**2011**).